Article citation info:
Mahmood T. O, Mohammed A. L, Antar R. K. Optimum disturbance-aware quantum-inspired dual-loop control of a chopper-fed dc motor drive. Diagnostyka. 2026;27(3):2026309. https://doi.org/10.29354/diag/231052.

DIAGNOSTYKA, 2026, Vol. 27, No. 3

e-ISSN 2449-5220
DOI: 10.29354/diag/231052

OPTIMUM DISTURBANCE-AWARE QUANTUM-INSPIRED DUAL-LOOP CONTROL OF A CHOPPER-FED DC MOTOR DRIVE

Omar Talal MAHMOOD *, **Laith Akram MOHAMMED**, **Rakan Khalil ANTAR**

Northern Technical University, Al-Minassa St., Mosul City, Nineveh Governorate, Iraq
* Corresponding author, e-mail: omar.talal@ntu.edu.iq

Abstract

This paper proposes a disturbance-aware quantum-inspired control (DAQIC) algorithm for speed control of a chopper-fed separately excited DC motor drive using a cascaded two-loop speed-current control structure. The suggested approach handles the limitations of typical PI control caused by load torque fluctuations, DC-link voltage variation, armature resistance variations, and measurement noise. In the outer speed loop controller, normalized speed error and error rate change data are mapped to probability-like conservative and aggressive control weight values. In the inner current loop controller, a feedforward duty-cycle term extracted from the motor armature voltage equation is merged with a bounded quantum-inspired correction control. A voltage-aware feasible reference limiter approach is also initiated to prevent the controller from generating unreachable speed commands during voltage sags and high-load conditions. The proposed controller is analysed through MATLAB-based simulations under nominal and disturbed operating conditions, and the results are compared with those of a conventional PI dual-loop controller. The results demonstrate that the proposed method enhances feasible-reference tracking, eliminates excessive current deviation, and improves robustness under constrained operating conditions. These findings show that the proposed DAQIC algorithm offers a practical and efficient control framework to control the speed for chopper-fed DC motor drive applications.

Keywords: chopper-fed drive, feasible-reference tracking, parameter variation, step response optimization, quantum-inspired control.

List of Symbols/Acronyms

Symbols	Meaning
DAQIC	Disturbance-Aware Quantum-Inspired Controller
DC	Direct Current
EMF	Electromotive Force
IAE	Integral of Absolute Error
ISE	Integral of Squared Error
ITAE	Integral of Time-weighted Absolute Error
MAE	Mean Absolute Error
PI	Proportional-Integral
PWM	Pulse-Width Modulation
QIC	Quantum-Inspired Controller

1. INTRODUCTION

High-performance electric motor drives are essential in industrial, transportation, robotic, and automation applications where accurate speed regulation, fast transient response, and robustness against operating disturbances are required. Among different motor-drive systems, DC motor drives remain an important platform for control research because of their simple structure, favourable torque–speed characteristics, and direct relationship between armature voltage and speed. Although modern AC and brushless drives are widely used, separately excited DC motors are still valuable for developing and validating advanced control strategies, as their speed-control theory can be readily extended to other drive systems. Previous studies indicate that DC drives continue to be utilized in many industrial applications due to their simplicity, reliability, and ease of implementation; for instance, PMDC motors offer favourable electrical properties for accurate wire feeding [1], and resonant inverters combined with DC drives yield excellent performance-to-cost ratios [2].

Received 2026-06-02; Accepted 2026-08-12; Available online 2026-08-19

In chopper-fed DC motor drives, the DC–DC converter regulates the average armature voltage by controlling the duty cycle of the switching signal [3]. This control confirms the chopper as an effective interface between the DC source and the motor, granting precise speed control up to the rated speed. Power-electronic drive references verify that switch-mode conversion provides superior efficiency compared with linear regulation approaches[4]. Moreover, recent experimental valuations exhibit that advanced pulse-width modulation (PWM) strategies, including quantum-inspired PWM, can dynamically control the average output voltage for these converters. Simultaneously, filtering lessens ripple components and magnetite energy consumption [5] [6], [7]. Particularly, DC motor drives and converter-fed systems are commonly analysed in terms of armature-current ripple, switching modes, and drive operational limits [6], [7].

Standard proportional–integral (PI) control continues to be one of the most dominant strategies for DC drive speed regulation due to its structural simplicity and practical implementation ease. In a classical chopper-fed, separately excited DC motor drive, the controller computes the speed deviation to generate the chopper firing control pulses, consequently modulating the duty cycle value and accordingly change the armature voltage. Prior literature on PI-controlled chopper-fed DC drives often uses a two-loop structure comprising an outer speed loop controller and an inner current loop controller. It has evaluated the entire system in MATLAB/Simulink. Within industrial motor-control strategies, a cascaded two-loop structure is widely implemented, comprising an inner current loop to control the rapid electrical response and an outer loop to regulate the slower electromechanical performance. Within this approach, the outer loop computes the speed deviation to generate the chopper gating signal from the inner loop, consequently adjusting the duty ratio and applied armature voltage. Notwithstanding these merits, fixed-gain PI controllers show significant performance deterioration when the drive is exposed to multiple simultaneous disturbances performance, such as load torque variations, DC-link voltage sags, armature resistance fluctuations, and measurement noise [1]. As a result, classical fixed-gain PID controllers frequently prove inadequate for regulating highly nonlinear motor systems during dynamic load shifts and other types of disturbances [7].

In these demanding operational conditions, the controller must not only reduce reference-tracking deviations but also firmly adhere to the drive's physical voltage and current constrains. Therefore, it is imperative to develop an adaptive control strategy—capable of responding to parameter uncertainties and nonlinear system dynamics—that can modulate its control action according to the severity of the speed error while enforcing strict duty-ratio saturation limits and feasible speed-reference tracking [8] [9], [10].

Quantum-inspired algorithms suggest a compelling conceptual structure for this adaptive decision-making [10]. These systems leverage probabilistic state vectors inspired by quantum bits, superposition, and quantum gates, yet remain entirely executable on conventional digital computers [8]. Seminal research by Han and Kim presented quantum-inspired evolutionary algorithms employing Q-bit encoding systems and Q-gates, indicating that probabilistic representation advances search heterogeneity and balances exploration and exploitation —a concept successfully applied to fast speed control in motor drives [11]. Subsequent literature has highlighted that these systems do not rely on physical quantum architectures; instead, they computationally emulate quantum phenomena such as qubits, interference, and superposition to augment algorithmic search and adaptive tracking abilities [12]. Topological optimization studies have further established that qubit-like variables can be represented by probability amplitudes and updated using quantum-inspired operations before decision selection and making, enabling complex optimization contexts to function purely mathematically without physical quantum computers [13], [14].

Leveraging these conceptual frameworks, many advanced control strategies and optimization methods have recently been proposed to moderate the nonlinearities and disturbances endemic to motor drive systems. To provide a detailed overview of the current state of the art, Table 1 establishes the primary topologies, controllers, and comparative outcomes of recent prominent studies in this domain.

As listed in Table 1, while a variety of adaptive and quantum-inspired controllers have been successfully applied within motor drives and energy management systems, a significant research gap persists. Most existing quantum-inspired topologies either introduce excessive computational burden—rendering them unfeasible for conventional microcontrollers—or decline to explicitly account for physical drive constraints, such as instantaneous voltage sags. To address this gap, this paper introduces a disturbance-aware quantum-inspired control (DAQIC) approach specifically designed for a chopper-fed, separately excited DC motor drive. The performance of this controller is rigorously evaluated across nominal and disturbed scenarios—including load torque step transients, DC-link voltage variations, armature resistance drift, and measurement noise—yielding significant reductions in integral error indices and current fluctuations compared to conventional PI control. Figure 1 shows the circuit diagram of a separately excited DC motor drive.

Although several studies have applied PI, fuzzy [15], adaptive, and quantum-inspired techniques to electric motor drives, most existing approaches focus either on controller-gain tuning, PWM generation, or optimization-based speed regulation. These methods generally do not explicitly account for the physical voltage limitation of the chopper, the duty-cycle constraint, the load-torque effect, and the armature-resistance variation in the speed-reference generation process. Therefore, their speed controllers may continue to demand an operating point that becomes physically unreachable during voltage sag or high-load operation. The scientific novelty of this work lies in developing a disturbance-aware quantum-inspired dual-loop controller in which the quantum-inspired law is not used as an isolated tuning mechanism but is embedded within a physically constrained chopper-fed DC motor drive framework. The proposed method combines a voltage-aware feasible speed-reference limiter, a feedforward-assisted current loop, and a bounded probability-weighted quantum-inspired correction mechanism. This integration allows the controller to distinguish between true tracking error and physically infeasible reference demand, thereby improving feasible-reference tracking and current regulation under simultaneous electrical, mechanical, and measurement disturbances.

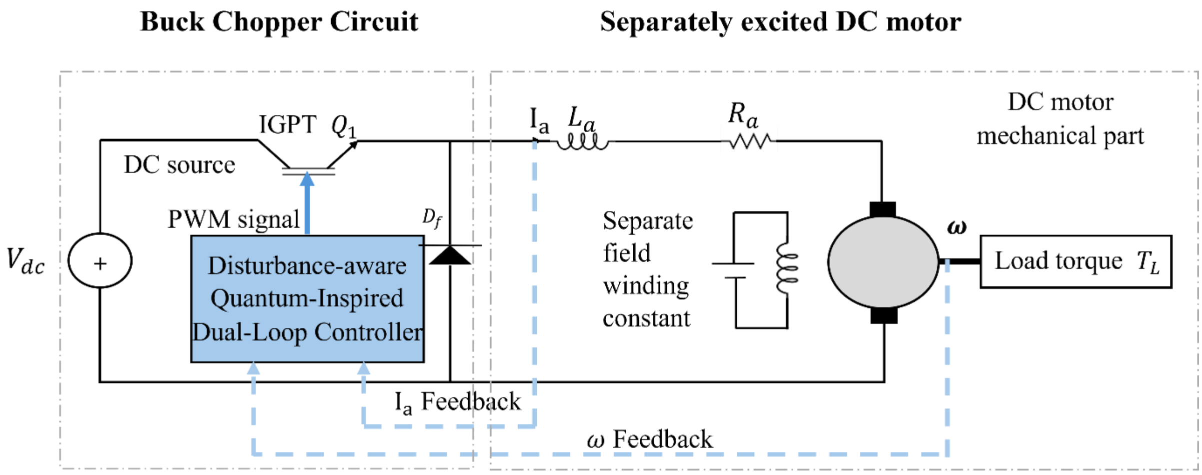

Fig. 1. Separately excited DC motor drive.

Table 1. Comparative analysis of recent control strategies and optimization topologies in electric motor drives and related systems

Ref.	Application Area	Topology & Controller	Key Advantages & Outcomes	Limitations & Complexity
		I. DC & PMDC Motor Drives		
[1]	PMDC Wire Feeding (GMAW)	High-Freq PWM / Sensorless Back-EMF	Highly accurate wire feed rates up to 5.7 kHz; eliminates the need for physical speed sensors.	Requires discontinuous conduction mode; imposes strict limits on maximum pulse width.
[2]	DC Motor Drive	QSRI / Predictive Resonant Current (OPRC)	Near-zero switching losses and low EMI enable full 4-quadrant motor operation.	Extremely constrained switching (zero-crossing only); requires complex-sampled-data modeling.
[7]	DC Motor (Theoretical)	QPWM via Real-Number Quantum Comparator	Formulates the mathematical theory and the novel quantum gate logic (Anti-CCNOT) for evaluating continuous signals.	Physical realization relies heavily on the theoretical stability of quantum logic gates.
[6]	DC Motor (Experimental)	Microcontroller-implemented QPWM	Achieves classical PWM precision in physical hardware while reducing overall energy consumption.	Emulating quantum probability required slightly higher microcontroller switching frequencies.
[8]	PLC DC Motor	Profibus-DP Network / Adaptive Fuzzy PID	Faster response and smaller overshoots under varying loads without rigid mathematical models.	Fuzzy rules rely heavily on expert experience; standard PLCs face multi-link delay challenges.
[16]	PMDC Chaos System	Boost Converter / CSO-tuned FFOC	Suppresses bifurcations; achieves a stable period-1 trajectory with lower steady-state error.	High structural complexity; standalone CSO requires a fuzzy layer to prevent load oscillation.
		II. AC, IM, & PMSM Drives		
[11]	IM Fast Speed Control	FOC / QEA-tuned PI + CRTRL Flux Estimator	Superior transient dynamics; CRTRL eliminates DC drift in flux estimation.	High algorithmic overhead due to the parallel maintenance of Q-bit and binary populations.
[12]	PMSM Speed Control	3-phase VSI / QSVPWM	Reduces RMS speed errors (0.47%) and THD; executes	Physical realization is highly dependent on the stability and maturity of quantum computing hardware.

			control sequences exponentially faster.	
[13]	IM Speed Control	3-phase VSI / QLSA-based Fuzzy (QLSAF)	Superior transient response and reduced MAE/RMSE; dynamically tunes membership functions.	Without QLSA, standalone fuzzy systems are inefficient and require extensive trial-and-error.
[17]	IM Position Control	FOC / NFTSMC + ABC-tuned Adaptive QNN	Excellent tracking and torque regulation; highly robust against temperature/load variations.	Structurally complex; requires three nested loops and continuous tuning of fractional parameters.
[18]	Smart EV IM Drive	Cuk Converter / Passivity-Based ETEDPOF	Tracks speed/torque variations globally over seconds; Cuk converter minimizes switching losses.	Continuous conduction mode is strictly required and necessitates complex nonlinear modeling.
		III. Electric Vehicles & Energy Management		
[9]	EV Controller Tuning	DC Motor Cart / Adaptive PID (WOA+BE+QAA)	Minimized overshoot and energy emissions; responds instantly to parameter drift.	Evolutionary algorithms require dense function evaluations, challenging standard real-time processors.
[19]	EV Charging Systems	Buck-Boost DC-DC / GGO + QCNN	Reduced hydrogen consumption (8.7%); achieves 99.97% energy management accuracy.	Requires continuous multi-objective fitness evaluation; high computational design complexity.
[20]	EV Energy Strategy	DS integrated with EVCS / Quantum VultureNet	Identifies near-global optimal solutions; manages multi-objective constraints, such as PV uncertainty.	Addressing optimization conservatism requires complex dynamic opposition-based learning.
		IV. Alternative Systems & Optimization		
[10]	Nonlinear Systems	Wheeled Robot / Adaptive QNN-PID	Compact 3-6-3 structure (only 30 parameters); rapid convergence guaranteed by Lyapunov criteria.	Highly susceptible to actuator noise if the plant sensitivity function is poorly estimated.
[14]	DC Arc Parameter ID	Fault Detection / Chaotic QCS	Highly accurate tracking of static nonlinear characteristics; avoids local optima spaces.	Chaotic local search mechanisms significantly increase computational overhead per iteration.
[21]	Marine Optimization	General Benchmarks / Marine Predators (MPA)	Simple implementation mimicking foraging patterns; outperforms standard GA/PSO models.	Prone to premature convergence in high-dimensional problems without fractional calculus hybridization.
[22]	EEG Classification	Signal Processing / QSVM	Harnesses quantum principles to process high-dimensional features; minimizes data complexity.	Constrained by NISQ hardware limitations and relies on complex pre-processing (VMD, SFS).
[23]	Quantum Internet	Network Nodes / MZI + SNSPD Detectors	Demonstrated 44 km teleportation fidelity (~98%); integrates with existing telecom fiber.	Sensitive to environmental drift; excess loss degrades signal-to-noise ratio over long distances.

2. PAPER CONTRIBUTIONS

The main contribution of this work is the development of a disturbance-aware quantum-inspired dual-loop controller for a buck-chopper-fed separately excited DC motor drive operating under practical electrical and mechanical constraints. The proposed controller is built around a cascaded speed-current structure but differs from a conventional PI-based design by incorporating a voltage-aware feasible speed-reference mechanism and a feedforward-assisted current-control loop. The feasible-reference mechanism is obtained from the steady-state voltage and torque relations of the DC motor, using the available DC-link voltage, duty-cycle limit, armature resistance, and estimated load torque to prevent the speed loop from demanding an operating point that cannot be physically reached during voltage sag, load increase, or resistance variation. In the inner loop, the feedforward term provides the main duty-cycle command from the motor voltage equation, while the quantum-inspired current controller supplies only a bounded corrective action to compensate for current-tracking errors and unmodelled disturbances. The quantum-inspired law uses normalized error and error-rate information to adjust the balance between conservative and aggressive control actions through sine-squared and cosine-squared weighting functions. To improve practical operation, the controller also includes speed-feedback filtering, reference filtering, asymmetric current reference rate limiting, duty-cycle saturation, and conditional anti-windup. The effectiveness of the proposed method is evaluated under nominal operation, load torque disturbance, speed-reference variation, DC-link voltage change, armature resistance variation, speed-measurement noise, and combined disturbances, with the results compared against a conventional dual-loop PI controller using time-response indices and integral error measures.

3. METHODOLOGY AND MATHEMATICAL REPRESENTATION

The proposed control system was implemented as a disturbance-aware quantum-inspired dual-loop

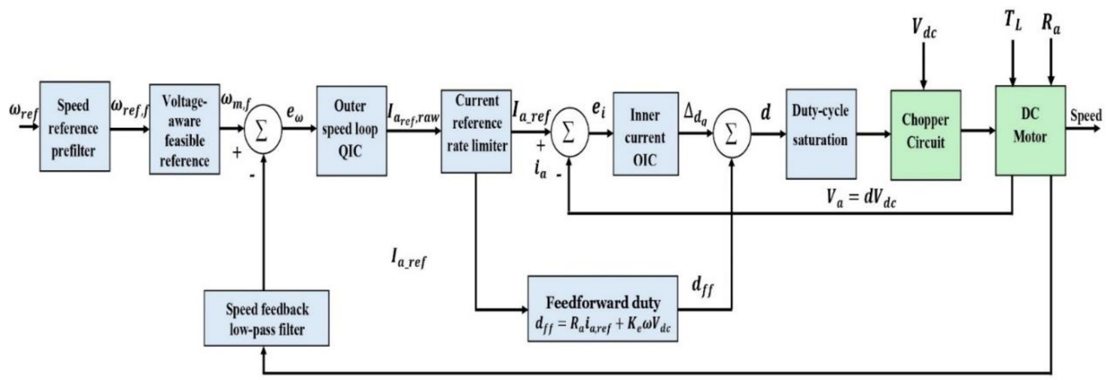

Fig. 2. Simplified Block diagram of the proposed quantum-inspired dual-loop control structure for the chopper-fed separately excited DC motor drive

controller for a chopper-fed separately excited DC motor. The outer loop regulates the motor speed and generates the reference armature current, whereas the inner loop regulates the armature current and generates the chopper duty cycle. The motor was represented using the standard armature electrical equation, the back-EMF equation, the electromagnetic torque equation, and the mechanical motion equation. The DC-DC chopper was modeled using the average voltage relation $V_a = dV_{dc}$. To improve robustness under combined disturbances, a voltage-aware feasible speed reference was introduced. The maximum achievable speed was estimated from the available DC-link voltage, duty-cycle limit, armature resistance, viscous friction, and estimated load torque. Therefore, the speed reference applied to the quantum-inspired speed controller (QIC) was limited to a physically feasible value during voltage sag or high-load operation. The proposed quantum-inspired controller uses normalized error and error-rate information to construct probability-amplitude-inspired weights based on $\sin^2(\theta)$ and $\cos^2(\theta)$. These weights blend conservative and aggressive control actions using a superposition-inspired control law. In the inner loop, a feedforward duty-cycle component was derived from the motor electrical equation, while the quantum-inspired current controller generated only a bounded correction term. This structure improves current tracking, reduces duty-cycle saturation, and enhances speed recovery under disturbances in load torque, input voltage, armature resistance, and measurement noise. The methodological novelty of the proposed DAQIC framework lies in integrating three elements into a single cascaded control architecture. First, the voltage-aware feasible reference limiter uses the available DC-link voltage, duty-cycle limit, armature resistance, and estimated load torque to prevent the speed loop from demanding physically unreachable operating points. Second, the inner current loop does not rely only on a feedback controller to generate the full duty cycle; instead, a feedforward duty-cycle term is derived from the motor armature voltage equation, while the quantum-inspired controller produces only a bounded correction. Third, the same probability-weighted, quantum-inspired law is used in both the speed and current loops to blend conservative and aggressive control actions based on normalized error and error rate values. Therefore, the proposed method is not simply a replacement for PI control; it is a constraint- and disturbance-aware control framework specifically designed for chopper-fed motor drives.

Figure 2 shows the simplified block diagram for this paper.

3.1. Mathematical Model of the Chopper-Fed Separately Excited DC Motor

The chopper-fed separately excited DC motor is represented using the conventional armature electrical equation and the mechanical motion equation [24][25],[26]. The average armature voltage supplied by the buck chopper is expressed as $V_a = dV_{dc}$, where d is the duty cycle and V_{dc} is the DC-link voltage. Accordingly, the motor dynamics can be written as:

$$
\begin{aligned}
i_a &= \frac{dV_{dc} - R_a i_a - K_e \omega}{L_a} \\
\dot{\omega} &= \frac{K_t i_a - T_L - B\omega}{J}
\end{aligned} \tag{1}
$$

where i_a is the armature current, R_a and L_a are the armature resistance and inductance, K_e is the backEMF constant, K_t is the torque constant, ω is the rotor speed, T_L is the load torque, J is the inertia, and B is the viscous friction coefficient. For the discrete-time simulation, the model is updated using the forward Euler method with sampling time T_s [1],[27] [24].

$$
\begin{aligned}
i_a(k+1) &= i_a(k) + T_s i_a(k) \\
\omega(k+1) &= \omega(k) + T_s \dot{\omega}(k)
\end{aligned} \tag{2}
$$

To keep the simulation consistent with practical drive limits, the duty cycle and armature current are constrained as [28], [29] [30]:

$$0 \le d \le d_{\max} \quad \text{and} \quad -i_{a,\max} \le i_a \le i_{a,\max} \tag{3}$$

In this study, the duty-cycle limits are selected as $d_{\min} = 0$ and $d_{\max} = 0.95$. The upper limit is kept below unity to avoid an idealized full-duty switching condition and to better represent the practical operating range of the buck chopper. Figure 3 presents the equivalent armature circuit together with the corresponding governing equations for easier reference.

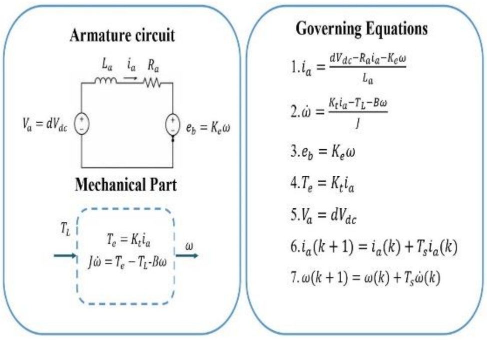

Fig. 3. Equivalent circuit and compact summary of the DC motor mathematical model

3.2. Disturbance-Aware Speed Reference and Feedback Processing

To improve the robustness of the proposed controller against measurement noise and sudden reference changes, first-order filtering is applied to both the measured speed and the speed reference [31][32]. The measured speed is expressed as the actual motor speed in rpm with an added noise component:

$$\omega_m(k) = \omega_{rpm}(k) + n_\omega(k) \tag{4}$$

where $n_\omega(k)$ represents the speed-measurement noise. In the proposed DAQIC controller, this measured signal is passed through a first-order low-pass filter before it is used in the speed loop. Similarly, the reference speed is filtered to avoid abrupt command changes that may lead to excessive current demand or duty-cycle saturation. These filtering stages are included only in the proposed DAQIC structure to support smoother and more robust operation under noisy and disturbed conditions. For a fair benchmark comparison, the conventional PI controller is evaluated using the same motor model and disturbance profiles, but without the additional DAQIC reference and feedback-processing stages.

3.3. Voltage-Aware Feasible Speed Reference Limiter

The voltage-aware feasible reference is introduced to avoid commanding a motor speed that cannot be reached under the available DC-link voltage and duty-cycle limit. Its derivation starts from the steady-state armature voltage equation and mechanical torque balance [1]:

$$V_a = R_a i_a + K_e\omega, K_t i_a = T_L + B\omega \tag{5}$$

Using these relations, the maximum achievable motor speed can be estimated from the available chopper voltage, armature resistance, viscous friction, and estimated load torque. Therefore, the feasible maximum speed is calculated as [29]:

$$\omega_{\max}(k) = \frac{d_{\max}V_{dc}(k) - R_a(k)\hat{T}_{L,f}(k)/K_t}{K_e + R_a(k)B/K_t} \tag{6}$$

The reference applied to the QIC speed loop is then limited as [33]:

$$\omega_{ref,lim}(k) = \min[\omega_{ref,f}(k), \gamma\omega_{\max,rpm}(k)] \tag{7}$$

where $\gamma = 0.97$ is used as a safety margin. This limiter is important because, during voltage sag, increased armature resistance, or high load torque, the original speed command may become physically unattainable. By reducing the reference to a feasible value, the controller avoids excessive duty-cycle saturation and prevents the speed loop from demanding an unreachable operating point.

3.4. Outer Speed-Loop QIC for Armature Current Reference Generation

In the proposed cascade control structure, the outer loop regulates the motor speed and generates the armature current reference for the inner current loop [1]. This structure is suitable for DC motor drives because the electromagnetic torque is directly related to the armature current. Therefore, the output of the speed controller can be treated as the required current command needed to reduce the speed-tracking error.

The speed error is calculated using the limited feasible reference and the filtered speed feedback:

$$e_\omega(k) = \omega_{\text{ref,lim}}(k) - \omega_{fb}(k) \tag{8}$$

The corresponding speed-error derivative is computed as [2]:

$$\dot{e}_\omega(k) = \frac{e_\omega(k) - e_\omega(k-1)}{T_s} \tag{9}$$

These two signals are then supplied to the outer quantum-inspired controller, which generates the raw armature current reference [34],[35]:

t the torque-producing current according to the

$$i_{a,\text{ref},\text{raw}}(k) = QIC_\omega[e_\omega(k), \dot{e}_\omega(k)] \tag{10}$$

To maintain safe operation and avoid unrealistic current commands, the final current reference is restricted within the allowable current-reference range [28]:

$$i_{a,\text{ref},\min} \le i_{a,\text{ref}}(k) \le i_{a,\text{ref},\max} \tag{11}$$

This outer-loop design allows the proposed controller to adjus speed error while still respecting the physical current limits of the drive.

3.5. General Quantum-Inspired Control Law Used in Both Loops

The same quantum-inspired control structure is used in the outer speed loop and the inner current loop. In each loop, the controller receives the error $e(k)$, the error derivative $\dot{e}(k)$, and the integral state $I(k)$. To keep the controller response bounded, the error and error derivative are first normalized as [34]:

$$x = \min(|e|/E_s, 1), x_d = \min(|\dot{e}|/\dot{E}_s, 1) \tag{12}$$

where E_s and $\dot{E}_s$ are scaling factors for the error and error derivative, respectively. The normalized error is then shaped using the parameter α, and the quantum-inspired weighting angle is calculated as:

$$\theta = \frac{\pi}{2}x^{\alpha}, P_A = \sin^2(\theta), P_C = \cos^2(\theta) \qquad (13)$$

Here, P_A and P_C represent the aggressive and conservative probability-like weights. When the error is small, the conservative component has more influence, while larger errors increase the contribution of the aggressive component.

The adaptive gain and bounded derivative term are defined as [34], [35]:

$$G_q = 1 + \lambda P_A + \eta x_d, \dot{e}_b = \dot{E}_x \tanh(\dot{e}/\dot{E}_x) \qquad (14)$$

where λ controls the influence of the aggressive weight, η adjusts the effect of the error-rate term, and $\dot{E}_x$ limits the derivative contribution. The bounded derivative is used to reduce excessive control action caused by sudden reference changes or measurement noise.

Two candidate control actions are then formed. The conservative action provides smoother behavior near the reference, while the aggressive action improves the response when the error is large:

$$\begin{gathered} u_C = K_{p,L}e + K_{i,L}I \\ u_A = K_{p,H}e + K_{i,H}I + K_{d,H}\dot{e}_b \end{gathered} \qquad (15)$$

The final controller output is obtained by blending these two actions through the quantum-inspired weights and applying the adaptive gain:

$$u = \mathrm{sat}\{G_q[P_C u_C + P_A u_A], u_{\min}, u_{\mathrm{ma}} \qquad (16)$$

The saturation limits ensure that the controller output remains within the allowable range. In the speed loop, this output corresponds to the armature current reference, while in the current loop it represents the duty cycle correction.

To avoid integrator windup during saturation, conditional integration is used [36]:

$$I(k+1) = \begin{cases} I(k) + T_s e(k), & \text{if integration is allowed} \\ I(k), & \text{otherwise} \end{cases} \qquad (17)$$

This structure allows the controller to respond strongly during large transients while maintaining smoother behavior near steady-state operation [37].

3.6. Asymmetric Current-Reference Rate Limiter for Torque-Stress Reduction

After the outer quantum-inspired speed controller generates the raw armature current reference $i_{a,\text{ ref, raw}}(k)$, an asymmetric rate limiter is applied before sending the command to the inner current loop. This step is included to avoid sudden changes in the current reference, which may otherwise produce high transient torque, large current stress, or duty-cycle saturation. In practical motor drives, the rising and falling rates of the current command may be selected differently because increasing the torque demand and reducing it do not necessarily require the same dynamic response.

When the current reference is increasing, the maximum allowed change is defined as [38],[39]:

$$\Delta i_{\max}^{+} = T_x R_i^{+} \qquad (18)$$

When the current reference is decreasing, the maximum allowed change is:

$$\Delta i_{\max}^{-} = T_n R_i^{-} \qquad (19)$$

where $R_i^{+}$and $R_i^{-}$are the rising and falling current-reference rate limits, respectively. The final limited current reference is then obtained as:

$$i_{a,ref,raw}(k) = \min[\max(i_{a,ref,max}(k)(k), i_{a,ref}(k-1) - \Delta i_{\max}^{-}), i_{\max,ri}(k-1) + \Delta i_{\max}^{+}] \qquad (20)$$

This limiter ensures that the current reference changes smoothly from one sampling instant to the next. As a result, the outer speed loop avoids demanding abrupt current jumps, while the inner current loop receives a more practical and physically achievable current command.

3.7. Inner Current-Loop QIC with Feedforward Duty-Cycle Compensation

The inner current loop regulates the armature current by adjusting the chopper duty cycle. The current error is calculated from the limited current reference and the measured armature current:

$$e_i(k) = i_{a,ref}(k) - i_a(k) \qquad (21)$$

The current-error derivative is then computed as:

$$\dot{e}_i(k) = \frac{e_i(k) - e_i(k-1)}{T_s} \qquad (22)$$

These two signals are applied to the inner quantum-inspired current controller, which produces a bounded duty-cycle correction:

$$\Delta d_q(k) = QIC_i[e_i(k), \dot{e}_i(k)] \qquad (23)$$

The correction term is limited to avoid excessive duty-cycle changes:

$$-d_{\mathrm{corr,max}} \le \Delta d_q(k) \le d_{\mathrm{corr,max}} \qquad (24)$$

In addition to this feedback correction, a feedforward duty-cycle term is calculated from the motor armature voltage equation [1]:

$$V_a = R_a i_a + K_{a\omega} \qquad (25)$$

Using the reference armature current, the desired feedforward armature voltage can be estimated as:

$$d_{ff}(k) = R_a(k) i_{a,m,f}(k) + K_c \omega(k) \qquad (26)$$

Therefore, the feedforward duty cycle is obtained as:

$$d_H(k) = \frac{R_{\mathrm{a}}(k) i_{\mathrm{s,nk/}}(k) + K_s \omega(k)}{V_{\mathrm{s}}(k)} \qquad (27)$$

The feedforward duty cycle is then saturated within the allowable duty-cycle range [28]:

$$d_{ff}(k) = \mathrm{sat}[d_{ff}(k), d_{\min}, d_{\max}] \qquad (28)$$

Finally, the applied chopper duty cycle is calculated by combining the feedforward duty with the quantum inspired correction:

$$d(k) = \mathrm{sat}[d_{ff}(k) + \Delta d_q(k), d_{\min}, d_{\max}] \qquad (29)$$

This structure reduces the burden on the quantum-inspired current controller. The feedforward term supplies the main duty-cycle command based on the motor model, while the QIC term only compensates for current-tracking errors and unmodeled disturbances. As a result, the inner loop becomes more physically interpretable and less dependent on large corrective control actions.

3.8. PI Benchmark Controller and Performance indices

A conventional cascaded PI controller is used as the benchmark for evaluating the proposed DAQIC method. The benchmark controller follows the same speed-current cascade structure, where the outer speed PI controller generates the armature current reference, and the inner current PI controller generates the chopper duty cycle. To ensure a fair comparison, both the PI controller and the proposed controller are evaluated under the same motor parameters, disturbance conditions, current limits, and duty-cycle constraints [28].The outer speed Pl controller is:

$$i^{PI}_{m,r\pi f}(k) = \text{sat}\left[K_{p\omega} e_{-}(k) + K_{i,} I_{-}(k), i_{ia,r\pi f,\text{ain}}, i_{a,r\pi f,\max}\right] \tag{30}$$

where $K_{p\omega}$ and $K_{i\omega}$ are the proportional and integral gains of the speed controller, $e_\omega(k)$ is the speed error, and $I_\omega(k)$ is the speed-loop integral state. The inner current PI controller then produces the duty-cycle command as:

$$d^{PI}(k) = \text{sat}\left[K_{pi} e_i(k) + K_{ii} I_i(k), d_{\min}, d_{\max}\right] \tag{31}$$

where K_{pi} and K_{ii} are the proportional and integral gains of the current controller, $e_i(k)$ is the armature current error, and $I_i(k)$ is the current-loop integral state.

The controller performance is assessed using standard time-domain response characteristics and integral error indices. The integral absolute error, integral squared error, and integral time-weighted absolute error are defined as:

The controller performance is assessed using standard time-domain response characteristics and integral error indices. The integral absolute error, integral squared error, and integral time-weighted absolute error are defined as:

$$IAE = \int_0^T |e_x(t)| dt$$
$$ISE = \int_0^T e_x^2(t) dt \tag{32}$$
$$ITAE = \int_0^T t|e_x(t)| dt$$

For the discrete-time simulation, these indices are approximated as:

$$IAE \approx \sum_{k-1}^{N} |e_s(k)| T_s$$
$$ISE \approx \sum_{k-1}^{N} e_s^2(k) T_s \tag{33}$$
$$ITAE \approx \sum_{k-1}^{N} t_k |e_s(k)| T_s$$

The armature current tracking deviation is calculated using the root-mean-square difference between the reference and actual armature current:

$$I_{dev} = \sqrt{\frac{1}{N}\sum_{k=1}^{N} \left[i_{a,ref}(k) - i_a(k)\right]^2} \tag{34}$$

The mean absolute speed error is also used to provide a direct measure of the average tracking error over the simulation interval:

$$MAE_\alpha = \frac{1}{N}\sum_{k-1}^{N} |e_\infty(k)| \tag{35}$$

3.9. Flowcharts and Implementation Procedure of the Proposed DAQIC Controller

Figure 4 presents the main flowchart of the MATLAB simulation for the chopper-fed DC motor drive, comparing the conventional PI controller with the proposed disturbance-aware quantum-inspired dual-loop controller. Figure 5 shows that, unlike a conventional single-loop speed controller, the proposed architecture combines a voltage-aware reference limiter, an outer QIC speed loop, an asymmetric current-reference rate limiter, an inner QIC current loop, and a feedforward duty-cycle term. This multifaceted structure allows the controller to accurately track the feasible speed reference while strictly respecting the physical voltage, current, and duty-cycle limits of the chopper-fed DC motor drive [40].

Finally, Figure 6 describes the general QIC block used in both loops. In the outer speed loop, the controller output is the raw current reference $i_{a,\text{ ref, raw}}$. In the inner current loop, the controller output is the quantum duty-cycle correction Δd_q. Therefore, the same QIC structure is efficiently reused by substituting the respective input errors, output saturation limits, and gain parameters.

3.10. Implementation Challenges and Tools Used

During the completion of this work, several modeling and implementation difficulties were encountered. The first challenge was to represent the chopper-fed DC motor drive under simultaneous electrical and mechanical disturbances, including load torque variation, DC-link voltage fluctuations, armature resistance changes, and speed-measurement noise. This behavior was addressed by developing a MATLAB-based discrete-time simulation model using the standard armature and mechanical equations of the DC motor together with the average buck-chopper voltage relation. The second challenge was that, during voltage sags and high-load operation, the original speed command could become physically unreachable due to limited DC-link voltage and duty-cycle saturation. To overcome this problem, a voltage-aware feasible speed-reference limiter was derived from the steady-state motor voltage and torque equations. The third challenge was maintaining stable current regulation without producing excessive transient current or duty-cycle oscillation. This response was handled using a feedforward duty-cycle term, a bounded quantum-inspired duty-cycle correction, asymmetric current-reference rate limiting, output saturation, and conditional anti-windup. Finally, measurement noise was mitigated using a first-order speed-feedback low-pass filter. At the same time, the controller performance was assessed using MATLAB-generated time-domain responses and quantitative indices, including rise time, settling time, overshoot, steady-state error, IAE, ISE, ITAE, current deviation, and mean absolute speed error.

4. SIMULATION RESULTS AND COMPARATIVE DISCUSSION

4.1.DC Motor, Chopper Circuit, and Controller Parameters

Table 2 lists the DC motor parameters used in this study to model the plant and to validate the proposed algorithm mathematically. In addition, Table 3 lists the chopper circuit specifications and the control saturation limits used to obtain the subsequent simulation results. The simulation was performed using a discrete-time average model of a buck-chopper-fed separately excited DC motor drive. The field excitation was assumed constant; therefore, the motor dynamics were represented by the armature voltage equation and the mechanical torque balance.

Table 2. DC motor parameters used in the simulation

Parameter	Symbol	Value/ unit	Justification
Armature resistance	R_a	5.79 Ω	Represents the nominal armature winding resistance used in the DC motor model.
Armature inductance	L_a	0.06 H	Represents the electrical energy-storage element of the armature circuit.
Torque constant	K_t	1.2 N.m/A	Converts armature current into electromagnetic torque.
Back-EMF constant	K_e	1.2 V.s/rad	Relates motor speed to generated back electromotive force.
Moment of inertia	J	0.012 Kg.m^2	Represents the equivalent rotor/load inertia.
Viscous friction coefficient	B	0.0204 N.m.s/rad	Models mechanical damping losses.
Rated speed	ω_{rated}	1250 rpm	Used as the main speed reference level in the simulation.
Rated current	I_{rated}	10A	Used as the main speed reference level in the simulation.
Maximum armature current	$i_{a,\,\max}$	25A	Defines the current saturation limit for safe operation.
Nominal DC supply voltage	$V_{dc,nom}$	220 V	Represents the rated DC-link voltage of the chopper drive.
Minimum duty cycle	$d_{\min}$	0	Lower physical switching limit.
Maximum duty cycle	$d_{\max}$	0.95	Upper duty limit used to avoid ideal 100% switching operation.

The buck chopper was modeled using the average voltage relation $V_a = dV_{dc}$, where the duty cycle was bounded between $d_{\min}$ and $d_{\max}$.

Table 3. Chopper and drive control limits

Parameter	Symbol	Value/unit
Nominal DC supply voltage	$V_{dc,\,\text{nom}}$	220 V
Minimum duty cycle	$d_{\min}$	0
Maximum duty cycle	$d_{\max}$	0.95
Minimum armature current reference	$i_{a,\,\text{ref}\,,\,\min}$	0 A

4.2. Simulation Scenarios, Input Data, and Assessment Criteria

The performance of the suggested disturbance-aware quantum-inspired controller was assessed through a MATLAB simulation of a chopper-fed, separately excited DC motor drive. The performance was strictly compared versus a typical PI two-loop controller under equal motor constraints, chopper limits, and disturbance scenarios.

Seven operational disturbance scenarios were evaluated: nominal operation, load torque step transients, speed-reference variation, input DC voltage fluctuation, armature resistance drift, speed-feedback noise perturbation, and combined disturbances. The comparison was carried out using both dynamic step-response indices and integral error indices, evaluating rise time, settling time, overshoot, steady-state error, IAE, ISE, ITAE, current deviation, and mean absolute speed error. This assessment validates the proposed controller's capability to enhance speed tracking, current regulation, and robustness under severely constrained and disturbed operating conditions. Table 4 summarizes the time sequence of the various types of disturbance occurrences during the simulation. The Noise in this case is active. Table 5 demonstrates the control parameters used in the suggested algorithm.

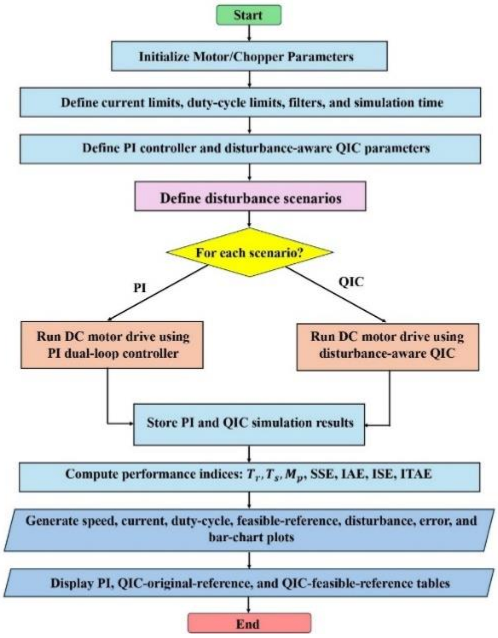

Fig. 4. Flowchart of the MATLAB code for the chopper-fed DC motor drive using the PI controller and the disturbance-aware quantum-inspired dual-loop controller

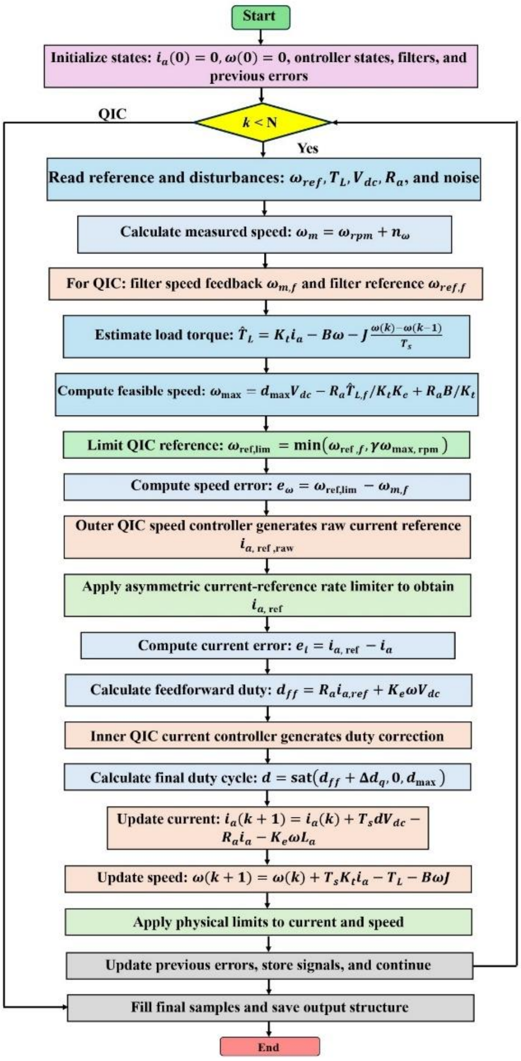

Fig. 5. Simulation-loop flowchart for the disturbance-aware quantum-inspired chopper-fed DC motor drive

Table 4. Combined disturbance case time sequence

Time interval (sec)	Speed reference ω_{ref} (rpm)	Load torque T_L(N.m)	DC voltage V_{dc}(V)	Armature resistance R_a (Ω)
$0 \le t < 1.5$	900	4	220	5.79
$1.5 \le t < 2.0$	1250	4	220	5.79
$2.0 \le t < 2.5$	1250	8	220	5.79
$2.5 \le t < 3.0$	1250	8	190	5.79
$3.0 \le t < 4.0$	1100	8	190	7.527
$t \ge 4.0$	1100	8	240	7.527

4.3. Speed Reference Response for Both PI and Disturbance-Aware Quantum Controllers

Figure 7 demonstrates the speed response of the DC motor under the mixed disturbance scenario using the conventional PI controller and the proposed disturbance-aware quantum-inspired controller. The original speed reference steps from approximately 900 rpm to 1250 rpm at t=1.5 s, and then reduces to 1100 rpm at t=3 s. The proposed controller also generates a voltage-aware, feasible QIC reference that is adaptively reduced during the voltage-limited interval. Both controllers follow the initial 900 rpm reference with stable transient performance. After the reference step-up at t=1.5 s, the proposed controller exhibits a faster but more oscillatory transient response, with a pronounced overshoot above 1250 rpm, while the PI controller tracks the reference with a smoother but slower transition. Around t=2s and t=2.5s, the combined disturbances become highly pronounced, remarkably in the quantum-inspired response, where transient speed dips occur before the controller rapidly recovers toward the commanded reference.

Table 5. Controller and simulation parameters

Parameter	Symbol	Value/unit	Justification
Sampling time	T_s	1×10^{-4}s	Provides sufficient resolution for the discrete-time motor drive simulation.
Minimum current reference	$i_{a,\text{ref},\text{min}}$	0 A	Prevents negative current reference in motoring operation.
Maximum current reference	$i_{a,\text{ref},\text{max}}$	22 A	Keeps current reference below the absolute current limit.
Current-reference rising rate	R_i^+	450 A/s	Limits sudden positive current-reference changes.
Current-reference falling rate	R_i^-	700 A/s	Allows faster current reduction during recovery.

Current-reference falling rate	R_i^-	700 A/s	Allows faster current reduction during recovery.
Speed-reference filter time constant	τ_{ref}	0.025 s	Reduces abrupt speed-reference transitions in DAQIC.
Speed-feedback filter time constant	τ_ω	0.010 s	Reduces speed-measurement noise effects in DAQIC.
Maximum quantum duty correction	$d_{\text{corr, max}}$	0.25	Bounds the duty-cycle correction generated by the inner QIC.
Feasible-reference safety margin	γ	0.97	Keeps the limited speed reference slightly below the estimated physical maximum.

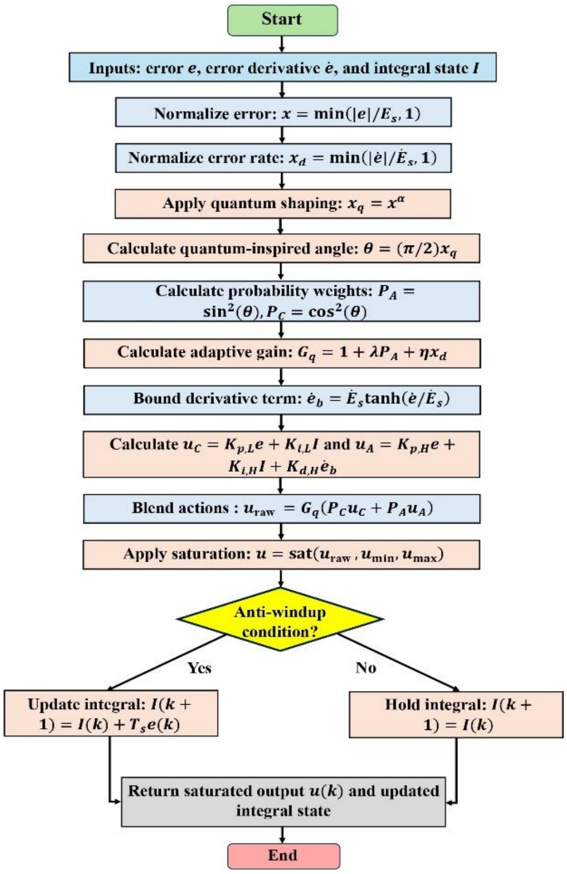

Fig. 6. Flowchart of the improved quantum-inspired controller with nonlinear quantum, bounded derivative action, adaptive gain, saturation, and anti-windup

The most crucial observation from Figure 7 is that the proposed controller does not simply compel the speed to follow the nominal reference when the drive becomes operationally constrained. During the interval in which the DC-link voltage decreases and the load/resistance conditions become more severe, the feasible QIC reference is dynamically reduced below the original speed command. This confirms that the voltage-aware reference limiter is active and prevents the controller from demanding an unattainable operating point. Therefore, the apparent deviation between the original reference and the actual QIC response should not be interpreted as poor tracking performance. Instead, it shows that the proposed algorithm respects the available voltage and duty-cycle limits of the chopper-fed drive system. After the DC-link voltage recovers near $t =$ 4s, the feasible reference returns close to the original command, and the motor speed rapidly converges to the desired operating point. reconverges with the original 1100 rpm command, and the proposed controller rapidly brings the motor speed back to the required operating point. This response confirms that the proposed controller keeps robust stability during bounded conditions, even though its transient response still shows overshoot and oscillation peaks that may demand further tuning of the quantum gains, the current-reference rate limiter, or the duty-correction threshold in future optimizations process.

4.4. Armature Current Regulation and Disturbance Rejection

Figure 8 describes the armature current behavior for the PI controller and the proposed DAQIC new algorithm under the combined disturbance operation. At the starting of the simulation, both controllers demonstrate a large transient current due to the motor starting from rest and requiring large electromagnetic torque for acceleration. After that, the armature current converges to a steady state of 5A during the first operating region. At t=1.5s, the reference speed increases from 900 rpm to 1250 rpm, resulting in a rapid rise in the generated reference current from the outer loop for speed. At $t = 2.0$s, the system is subjected to a load torque step change from 4 N·m to 8 N·m, causing another increment in the armature current to supply the additional load torque demanded by the motor. More complex current recovery action appears between $t = 2.5$s and $t = 3.5$s due to the simultaneous DC-link voltage reduction and an increase in the armature resistance. Throughout these constrained intervals,

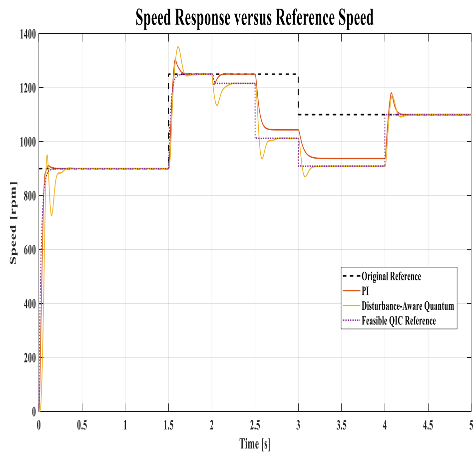

Fig. 7. Step response for speed reference of both pi and disturbance-aware quantum controllers

the quantum-inspired controller tightly tracks its dynamic current reference. At $t = 4.0$s, the DC-link voltage recovers from 190 V to 240 V, inducing a final transient surge in the armature current before stabilizing.

As shown in Figure 8, the proposed quantum-inspired inner loop ensures tight tracking of the dynamic current reference across the duration of the simulation, particularly after the major transients. The observed current transients are inherent physical responses, as the motor inherently draws elevated armature current during initial acceleration, during load steps, and during voltage recovery. Compared to the PI controller, the quantum-inspired controller exhibits a more pronounced transient correction action at specific disturbance events; however, it also displays swifter steady-state recovery and stable current tracking after each change. This robust response is primarily credited to the feedforward duty-cycle term, which generates the baseline voltage demanded by the motor. At the same time, the bounded quantum-inspired action effectively mitigates residual current-tracking deviation. Therefore, the results demonstrate the efficacy of the proposed inner current loop in regulating the torque-producing current under severe combined perturbations. While the controller demonstrates excellent tracking, the transient current transients could be further mitigated in future designs by retuning the current-reference rate limiter or modulating the high current-loop gain parameters.

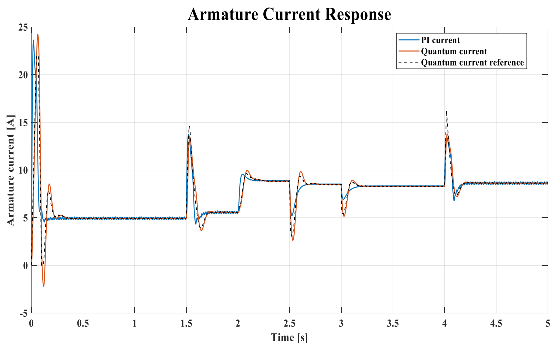

Fig. 8. Armature current response for both PI and QIC

4.5. Chopper Duty-Cycle Response and Saturation Behavior

Figure 9 depicts the chopper duty-cycle behavior under the combined disturbance case. During the initial starting phase, both controllers rapidly saturate the duty cycle to accelerate the motor. The duty cycle escalates again at $t = 1.5$ s due to the speed-reference step variation and then remains elevated during the load torque step and DC-link voltage sag periods. At $t = 4$ s, when the DC voltage regains 240 V, the necessary duty cycle likewise decreases.

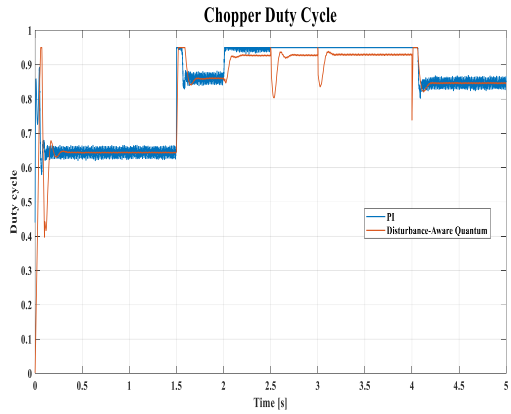

Fig. 9. Chopper duty cycle behaviour

The duty-cycle profile validates that the chopper effectively mitigates speed, load, and voltage disturbances by adjusting the applied armature voltage. Notably, during the voltage-sag period, both controllers operate nearby maximum modulation limit to keep target speed. Besides, the proposed DAQIC controller exhibits significantly smoother duty profiles across many operating regions compared to the PI benchmark. This stability is achieved due to the feedforward term provides the main duty command, while the quantum controller adds only a bounded correction. This performance firmly confirms and supports the efficiency of the feedforward-assisted inner-loop approach.

4.6. Feedforward and Quantum Correction Components of the Duty Cycle

Figure 10 shows the decomposition of the proposed quantum-controller duty cycle into three components: the total duty cycle, the feedforward duty, and the quantum correction. The feedforward duty is the main component and closely follows the total duty cycle throughout most of the simulation. In contrast, the quantum correction remains small and becomes more noticeable mainly during transient events, such as the initial startup, the reference step change at $t = 1.5$ s, the voltage-sag onset around $t = 2.5$ s, and the voltage recovery near $t = 4$ s.

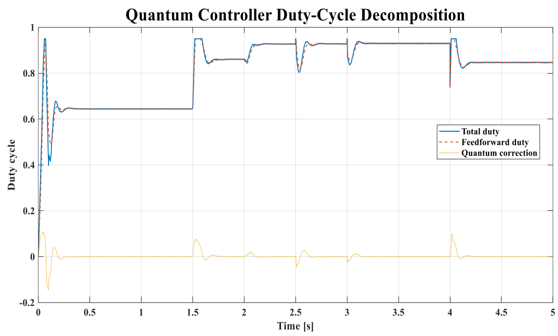

Fig. 10. Quantum controller duty cycle decomposition behaviour

This result confirms that the proposed inner current loop does not generate the full duty cycle using the quantum algorithm alone. Instead, the feedforward term provides the nominal voltage command based on the motor model, while the quantum correction compensates only for transient current-tracking errors and unmodeled disturbances. This structure is beneficial because it makes the controller more physically interpretable and avoids unnecessary quantum correction actions. The limited magnitude of the correction signal also confirms that the feedforward-assisted design reduces the control burden on the quantum controller.

4.7. Applied Load-Torque Disturbance Profile

Figure 11 shows the performance of the applied load torque disturbance used in the combined disturbance scenario. The motor initially operates under the rated load torque of (4 N.m) from $t = 0$s to $t = 2$s. At $t = 2$ s, a step-up load disturbance is initiated, abruptly increasing the load torque by 100% to (8 N·m). This high load torque is then sustained until the end of the simulation. This profile is used to rigorously evaluate the two controllers' ability to continue accurate speed regulation and current tracking when the mechanical load demand suddenly changes.

4.8. Speed-Tracking Error Under Combined Disturbances

Figure 12 illustrates the speed tracking change for both PI controller and the proposed DAQIC method under the simultaneous disturbance case. At the starting of the simulation, both controllers exhibit a significant initial error because the motor speed starts from zero while the reference speed is already 900 rpm. The error rapidly converges close to zero following the initial transient period. Distinct error excursions appear at $t = 1.5$ s due to the speed-reference step, at $t = 2$ s due to the load torque disturbance, and at $t = 4$ s due to the voltage recovery.

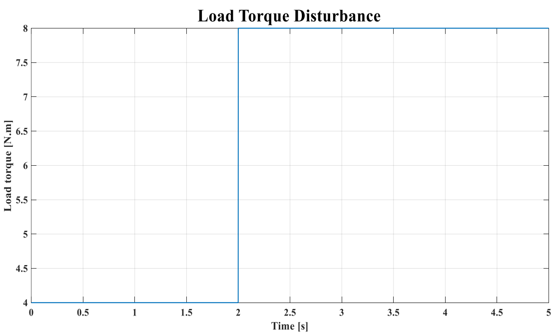

Fig. 11. Load torque disturbance behaviour

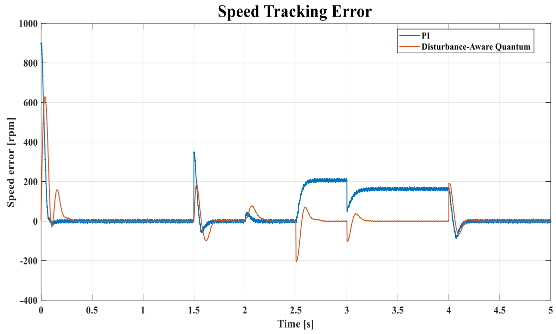

Fig. 12. Speed tracking error behaviour.

The PI controller shows a larger sustained positive error between $t = 2.5$ s and $t = 4$ s, indicating that it has difficulty maintaining speed regulation during the voltage-sag and high-load interval. In contrast, the quantum-inspired controller produces sharper transient error peaks around some disturbance instants, particularly near $t = 2.5$ s, but it recovers more quickly after each disturbance. This behavior demonstrates better feasible-reference tracking under constrained operation, mainly due to the voltageaware reference limiter and the feedforward-assisted current loop. Overall, the proposed controller reduces long-duration tracking errors, although further tuning of the quantum parameters may help reduce the transient spikes.

4.9. Input Voltage and Armature Resistance Disturbance Profiles

Figure 13 shows the profile of the input DC voltage and armature resistance fluctuations applied during the combined disturbance scenario scheme. The input DC-link voltage is initially kept at 220V from $t = 0s$ to $t = 2.5$ s. At $t = 2.5$ s, the voltage decreases to 190 V, implying a severe voltage-sag performance. Then, this voltage increased suddenly to 240 V at $t = 4$ s. Meanwhile, the armature resistance persists at its nominal value of approximately 5.79Ω until $t = 3$ s. After $t = 3$ s. After that, it rises to 7.53 Ω, to emulate factors such as thermal heating or physical resistance uncertainty.

4.10. Voltage Aware-Feasible Speed Reference Analysis

Figure 14 illustrates the voltage-aware feasible speed reference beside the original demanded speed reference and the measured quantum controller speed trajectory. The initial reference transitions from 900 rpm to 1250 rpm at $t = 1.5$ s, and then decreases to 1100 rpm at $t = 3$ s. During the simultaneous voltage-sag and high-load interval, the feasible reference becomes lower than the original speed reference, especially between $t = 2.5$ s and $t = 3$ s. In this period, the quantum-inspired controller follows the feasible reference instead of forcing the motor to track the original command, which is physically difficult to achieve under the available voltage and duty-cycle limits.

This behavior highlights the importance of the voltage-aware reference limiter. When V_{dc} drops to 190 V and the load demand remains high, the available armature voltage becomes insufficient to maintain the original speed reference without driving the duty cycle toward its upper limit. The situation becomes more constrained when the armature resistance increases, which further reduces the effective voltage available for speed production. Therefore, the proposed controller limits the reference to a feasible value and prevents excessive duty-cycle saturation. After the DC-link voltage recovers to 240 V at $t = 4$ s, the feasible reference returns close to the original command, and the motor speed quickly converges to the desired operating point. This proves that the proposed control structure follows the physical and electrical limits of the chopper-fed DC motor drive while sustaining stable speed regulation under constrained operating conditions.

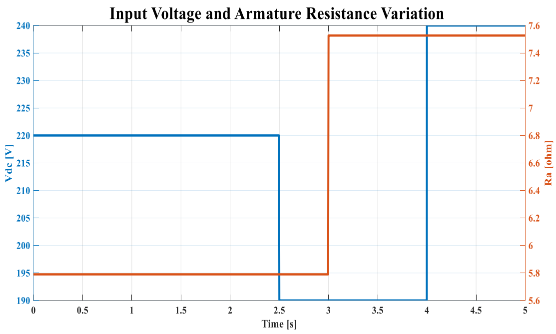

Fig. 13. Input voltage and armature current disturbance behaviour

4.11. Quantitative Performance Comparison Analysis: PI vs DAQIC

This subsection presents a quantitative comparison between the proposed DAQIC framework and the conventional PI controller. The evaluation considers seven operating conditions and includes the main step-response characteristics, speed-tracking error indices (IAE, ISE, and ITAE), current variation, and mean absolute speed error. This comparison specifies a stronger evaluation of the controller's performance under both nominal and disturbed operating scenarios.

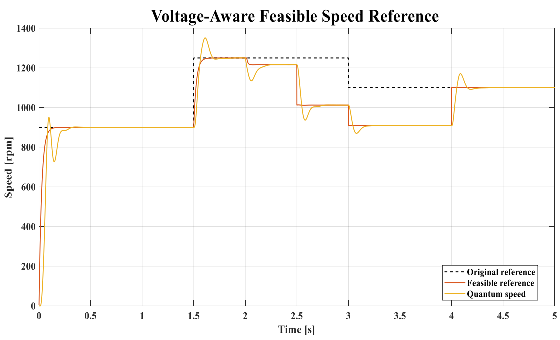

Fig. 14. Voltage-aware feasible speed reference response

4.11.1. Case 1: Nominal Motor Operation

In Table 6, a summary of the performance of the motor under nominal operating scenarios is provided, where no external disturbances are used. Both controllers (PI and QIC) accomplish zero steady-state error, revealing that both methods can track the reference speed precisely in normal operation. The proposed QIC specifies a slightly faster rise time of 0.0674 s compared with 0.0694 s for the PI controller. More importantly, it considerably reduces the overshoot from 1.2248% to 0.1308% and lowers the current ripple from 0.6878 A to 0.4343 A. This performance indicates that the QIC produces a smoother speed response with reduced current variation. However, the settling time of the QIC is longer, reaching 0.2474 s compared with 0.099 s for the PI controller. This slower settling response, together with the higher IAE and ITAE values, shows that the proposed controller behaves more conservatively after the initial transient. Nevertheless, this trade-off is acceptable because the main objective of the DAQIC is not only to optimize nominal-condition response, but also to improve robustness under constrained and disturbed operating conditions.

Table 6. Step response results for normal operation of the motor without disturbances

Metric	PI	QIC-original	QIC-feasible
Rise time [s]	0.0694	0.0674	0.0674
Settling time [s]	0.0990	0.2474	0.2474
Overshoot [%]	1.2248	0.1308	0.1308
SS error [rpm]	0.0000	0.0000	0.0000
IAE	58.8095	65.8158	65.8158
ISE	49304.3	85332.7	34883.5
ITAE	1.9018	5.5592	4.7842
Current deviation	0.6878	0.4343	0.4343
Mean abs speed error	11.7742	19.3878	13.1630

Case 2: Load Torque Step Disturbance

Table 7 collects the performance indices for a sudden disturbance in load torque change. The QIC-feasible algorithm succeeds a rapider rise time (0.0641s) compared to the PI equal (0.0694 s). Additionally, the QIC suppresses the current variation from 0.6939A to 0.4362A, confirming superior inner-current regulation. However, the PI controller delivers lesser IAE and ITAE metrics than the QIC-feasible result. The substantial steady-state error (34.3903 rpm) observed in the QIC-original column arises mathematically as the unconstrained reference collapses to account for the drive's physical limits after the motor load step.

Table 7. Step Response Results for Motor Speed Under Load Torque Step Disturbances

Metric	PI	QIC-original	QIC-feasible
Rise time [s]	0.0694	0.0674	0.0641
Settling time [s]	2.0472	NaN	2.1241
Overshoot [%]	1.2248	0.1308	2.9635
SS error [rpm]	0.0000	34.3903	0.0000
IAE	61.0187	206.8576	73.5953
ISE	49358.93	89740.9626	35304.7788
ITAE	6.4301	380.8162	20.9499
Current deviation	0.6939	0.4362	0.4362
Mean abs speed error	12.2160	41.3835	14.7188

4.11.3. Case 3: Speed Reference Change

Table 8 exhibits performance during a dynamic speed-reference variation. Both controllers effectively reach zero steady-state error. The QIC yields a marginally faster rise time (2.0079 s) versus the PI (2.0197 s), though the PI settles slightly faster (2.1117 s vs 2.1650 s). While the QIC exhibits a higher overshoot (8.4335% vs 4.0843%), the QIC-feasible framework significantly minimizes the ISE (15353.0083 vs 22019.8936) and drastically reduces current deviation (0.4811 A vs 1.0605 A).

Table 8. Step response results under speed reference change

Metric	PI	QIC-original	QIC-feasible
Rise time [s]	2.0197	2.0079	2.0079
Settling time [s]	2.1117	2.1650	2.1650
Overshoot [%]	4.0843	8.4335	8.4335
SS error [rpm]	0.0000	0.0000	0.0000
IAE	43.8199	83.8186	55.2216
ISE	22019.894	43147.6673	15353.0083
ITAE	26.4815	47.0641	31.9295
Current deviation	1.0605	0.4811	0.4811
Mean abs speed error	8.7728	16.7724	11.0441

4.11.4. Case 4: Input Voltage Variation

As detailed in Table 9, both controllers maintain a 0.0674 s rise time and zero steady-state error under input voltage variation. However, the DAQIC outperforms the PI benchmark by a wide margin. Overshoot is attenuated from 9.7107% to 2.7772%, settling time is slightly reduced, and current deviation is vastly improved (0.4558 A vs 8.8567 A). Furthermore, the QIC-feasible calculations cut the IAE by more than half (75.6973 vs 160.6192) and reduced the ITAE by nearly an order of magnitude (27.2818 vs 238.8374).

Table 9. Step response results under input voltage variation

Metric	PI	QIC-original	QIC-feasible
Rise time [s]	0.0674	0.0674	0.0674
Settling time [s]	3.1062	3.0929	3.0929
Overshoot [%]	9.7107	2.7772	2.7772
SS error [rpm]	0.0000	0.0000	0.000
IAE	160.6192	251.8540	75.6973
ISE	55887.92	100879.99	35382.6
ITAE	238.8374	358.1274	27.2818
Current deviation	8.8567	0.4558	0.4558
Mean abs speed error	32.1357	50.3823	15.1392

4.11.5. Case 5: Armature Resistance Variation

Table 10 validates performance under simulated parameter drift. The QIC yields a faster rise time (0.0674 s vs 0.0694 s) and drastically minimizes overshoot (0.1308% vs 1.2248%). While the PI exhibits a faster settling time, the QIC-feasible structure successfully minimizes the ISE metric. against thermal heating or resistance uncertainty. It decreases the current variation (0.4343A against 0.6890A) indicating robustness against thermal heating or resistance uncertainty.

4.11.6. Case 6: Speed Feedback Noise

Table 11 demonstrates that both controllers maintain minimal steady-state error under feedback noise. The QIC achieves a faster rise time and significantly attenuates overshoot (0.1406% compared to 1.2541% for PI). Furthermore, the QIC-feasible logic reduces the ISE and drastically cuts the current deviation (0.4358 A vs 0.8758 A), demonstrating that the adaptive quantum weights efficiently filter actuator noise.

4.11.7 Case 7: Combined Disturbances

Table 12 summarizes the results for the most severe test condition, simultaneous combined disturbances. The QIC achieves a faster rise time (1.4920 s vs 1.5034 s) and tighter steady-state regulation (0.0209 rpm error vs 0.0541 rpm). While the QIC exhibits a mathematically higher overshoot (22.8342% vs 18.4788%), this is substantially outweighed by its overall tracking superiority. The QIC-feasible framework drastically minimizes IAE (89.3681 vs 305.5232), ISE (18159.9815 vs 66271.6202), and ITAE (127.3980 vs 871.1872), while nearly eliminating large current deviations (0.5435 A vs 7.5799 A). Ultimately, the DAQIC framework demonstrates superior robustness and feasible reference tracking under extreme physical constraints.

The novelty of the proposed DAQIC method is also reflected in the obtained results. Unlike the PI controller, which attempts to track the original reference even when the motor drive becomes voltage-constrained, the proposed controller dynamically follows the feasible speed reference derived from the system's physical limitations. This behaviour is particularly important under DC-link voltage sag, increased load torque, and variations in armature resistance. Therefore, the improvement of the proposed method should not be evaluated only by classical original-reference tracking indices, but also by its ability to maintain feasible-reference tracking and stable current regulation under constrained operation.

Table 10. Step response results under armature resistance variation

Metric	**PI**	**QIC-original**	**QIC-feasible**
Rise time [s]	0.0694	0.0674	0.0674
Settling time [s]	0.0990	0.2474	0.2474
Overshoot [%]	1.2248	0.1308	0.1308
SS error [rpm]	0.0000	0.0000	0.0000
IAE	59.0020	96.8785	65.8158
ISE	49304.8745	85332.7266	34883.5526
ITAE	2.3909	5.5592	4.7842
Current deviation	0.6890	0.4343	0.4343
Mean abs speed error	11.8127	19.3878	13.1630

Table 11. Step response results under speed feedback noise

Metric	**PI**	**QIC-original**	**QIC-feasible**
Rise time [s]	0.0694	0.0674	0.0674
Settling time [s]	0.0995	0.2476	0.2476
Overshoot [%]	1.2541	0.1406	0.1406
SS error [rpm]	0.0753	0.0790	0.0790
IAE	59.9896	97.5544	66.4917
ISE	49306.5808	85339.5281	34890.2143
ITAE	4.9241	7.4317	6.6567
Current deviation	0.8758	0.4358	0.4358
Mean abs speed error	12.0102	19.5230	13.2981

Table 12. Step response results: speed under combined disturbances

Metric	**PI**	**QIC-original**	**QIC-feasible**
Rise time [s]	1.5034	1.4920	1.4920
Settling time [s]	4.1251	4.1304	4.1304
Overshoot [%]	18.4788	22.8342	22.8342
SS error [rpm]	0.0541	0.0209	0.0209
IAE	305.5232	427.7192	89.3681
ISE	66271.62	111696.6544	18159.9815
ITAE	871.1872	1127.2386	127.3980
Current deviation	7.5799	0.5435	0.5435
Mean abs speed error	61.1124	85.5511	17.8733

5. CONCLUSION

This paper presented a disturbance-aware quantum-inspired dual-loop controller for a chopper-fed separately excited DC motor drive. The proposed method integrates an outer quantum-inspired speed loop, an inner quantum-inspired current loop, a voltage-aware feasible reference limiter, and a feedforward-assisted duty-cycle generation mechanism. Unlike conventional PI control, the proposed controller considers the physical voltage and duty-cycle constraints of the chopper-fed drive, preventing it from demanding unreachable speed references during voltage sags, high load torque, or armature resistance variations. The main novelty of the proposed approach is that the quantum-inspired controller is integrated with the physical voltage and duty-cycle constraints of the chopper-fed drive, allowing the controller to track a feasible speed reference rather than forcing the motor to follow an unreachable command during constrained operation.

The proposed controller was evaluated under nominal operation, load torque variation, speed-reference change, input-voltage variation, armature resistance change, speed-feedback noise, and combined disturbances. The results demonstrate that the proposed DAQIC method improves feasible-reference tracking and armature-current regulation, especially under constrained operating conditions. Under nominal operation, the overshoot was reduced from 1.2248% using PI control to 0.1308% using DAQIC, while the current deviation was reduced from 0.6878 A to 0.4343 A. Under input-voltage variation, the proposed controller reduced the overshoot from 9.7107% to 2.7772% and decreased the current deviation from 8.8567 A to 0.4558 A. In the severe combined-disturbance case, the feasible-reference evaluation showed reductions of 70.8%, 72.6%, 85.4%, and 70.8% in IAE, ISE, ITAE, and mean absolute speed error, respectively, while the current deviation was reduced by 92.8%.

These results confirm the practical impact of the proposed controller for constrained DC motor-drive applications where the original speed command may become physically infeasible. The main contribution is not only the use of a quantum-inspired control law, but its integration with feasible-reference generation and feedforward duty-cycle correction. Future work will focus on switching-model validation, hardware-in-the-loop testing, real-time implementation, and systematic optimization of the quantum-inspired controller parameters.

The proposed DAQIC concept can be generalized to other systems with measurable feedback variables, actuator constraints, and a physical model for estimating a feasible reference or feedforward control action. For example, the same structure can be adapted to PMDC motor drives, BLDC and PMSM drives, DC-DC converter systems, inverter-fed motor drives, and other constrained electromechanical systems. In such applications, the outer-loop variable, inner-loop variable, actuator limit, and feedforward model should be redefined according to the specific plant. For instance, in a DC-DC converter, the voltage or current reference may replace the motor-speed reference, while duty-cycle saturation remains the actuator constraint. In an inverter-fed motor drive, the feasible reference may be derived from the available DC-link voltage, current limit, and torque requirement. Therefore, the generalization is possible, but it requires system-specific modeling, parameter tuning, and validation under the relevant disturbance conditions.

Source of funding: *No funding project.*

Author contributions: *research concept and design, O.T.M.; Collection and/or assembly of data, O.T.M., I.A.M.,R.K.A.; Data analysis and interpretation, O.T.M.; Writing the article, I.A.M. , R.K.A.; Critical revision of the article, I.A.M., R.K.A.; Final approval of the article, O.T.M., R.K.A.*

Declaration of competing interest: *The authors declare that they have no known competing financial interests or personal relationships that could have appeared to influence the work reported in this paper.*

REFERENCES

1. Paul AK. Robust PMDC motor control for accurate wire feeding in GMAW using back EMF. IEEE Trans Ind Electron. 2020; 67: 413-420. https://doi.org/10.1109/TIE.2019.2896131.
2. Gun WM, Jung HK, Hyun CC, Kwan YC, Myung JY. Quantum series resonant inverter for a DC motor drive. In: Proceedings of the 10th IEEE Region Conference on Computer, Communication, Control and Power Engineering. IEEE. 1993: 563-567. https://doi.org/10.1109/tencon.1993.320705.
3. Ramya Sri N, Kumar MP. An extended voltage gain three-level DC/DC bidirectional converter in an electric vehicle traction system. IEEE Access. 2025; 13: 146527-146556. https://doi.org/10.1109/access.2025.3600441.
4. Antar RK, Allu AA, Ali AJ. Sensorless speed control of separately excited DC motor using neuro-fuzzy controller. In: 2013 International Conference on Electrical Communication, Computer, Power, and Control Engineering. IEEE. 2013: 37-42. https://doi.org/10.1109/ICECCPCE.2013.6998767.
5. Negadi K, Boudiaf M, Araria R, Hadji L. Improvement of the amplification gain for a propulsion drives of an electric vehicle with sensor voltage and mechanical speed control. Smart Struct Syst. 2022; 29(5): 661-675. https://doi.org/10.12989/sss.2022.29.5.661.
6. Saidat S, Boumekhita R, Tadjine M, Zioui N. Experimental assessment of quantum PWM performance in DC motor speed control applications. In: 2025 International Conference on Decision Aid Sciences and Applications. IEEE. 2025: 970-975. https://doi.org/10.1109/DASA68193.2025.11498904.
7. Saidat S, Boumekhita R, Tadjine M, Zioui N, Quantum pulse-width modulation design and implementation for a DC motor drive, Quantum Inf. Process. 23 (2024) 1–24. https://doi.org/10.1007/s11128-024-04284-2.
8. Zhu H. Research on PLC DC motor speed control system based on quantum fuzzy control algorithm. In: Proceedings - International Conference on Applied Artificial Intelligence and Computing. IEEE. 2022: 1672-1675. https://doi.org/10.1109/ICAAIC53929.2022.9793235
9. Mohamed MT, Alkhalaf S, Senjyu T, Mohamed TH, Elnoby AM, Hemeida AM. A hybrid evolutionary approach for electric vehicle controller tuning: integration of WOA, QAA, and RMSProp. Results Eng. 2025; 27: 106389. https://doi.org/10.1016/j.rineng.2025.106389.
10. Hanna YF, Khater AA, El-Bardini M, El-Nagar AM. Real-time adaptive PID controller based on quantum neural network for nonlinear systems. Eng Appl Artif Intell. 2023; 126: 106952. https://doi.org/10.1016/j.engappai.2023.106952.
11. Md. Habibullah, Md. A. Hossain, Md. A. Rafiq, and B. C. Ghosh. Quantum evolutionary algorithm based fast speed controlled induction motor drive with CRTRL flux estimator. In: International Conference on Electrical and Computer Engineering. IEEE. 2010:478-481. https://doi.org/10.1109/icelce.2010.5700733.
12. Zioui N, Mahmoudi A, Fazilat M, Kone O, Dermouche R, Tadjine M. Quantum space vector pulse width modulation for speed control of permanent magnet synchronous machines. e-Prime Adv Electr Eng Electron Energy. 2025; 13: 101074. https://doi.org/10.1016/j.prime.2025.101074.
13. Ali JA, Hannan MA, Mohamed A, Jern KP, Abdolrasol MG. Implementation of DSP-based optimal fuzzy logic speed controller for IM drive using quantum lightning search algorithm. Measurement. 2020; 153: 107372. https://doi.org/10.1016/j.measurement.2019.107372.
14. Yin Z, Wang L, Zhang Y, Gao Y. Parameter identification of DC arc models using chaotic quantum cuckoo search. Appl Soft Comput. 2021; 108: 107451. https://doi.org/10.1016/j.asoc.2021.107451.
15. Bouradi S, Negadi K, Araria R, Boumediene B, Koulali M. Design and implementation of a four-quadrant DC-DC converter based adaptive fuzzy control for electric vehicle application. Math Model Eng Probl. 2022; 9(3): 721-730. https://doi.org/10.18280/mmep.090319.
16. Moustafa E, Abou-Zalam B, Sobaih AA, Nabil E, Sayed A. Optimized fuzzy fractional-order controller for a nonlinear chaos system with period-doubling bifurcation

analysis. Int J Control Autom Syst. 2023; 21: 3492-3503. https://doi.org/10.1007/s12555-022-1020-9.
17. Zirkohi MM. Fast terminal sliding mode control design for position control of induction motors using adaptive quantum neural networks. Appl Soft Comput. 2022; 115: 108268. https://doi.org/10.1016/j.asoc.2021.108268.
18. Arathy Rajeev VK, Valsalal P. ETEDPOF gain optimization for Cuk converter fed induction motor coupled with DC motor for smart EV. In: International Conference on Trends in Engineering Systems and Technologies. IEEE. 2025: 1-6. https://doi.org/10.1109/ICTEST64710.2025.11042875.
19. Rajendar G, Kumar BV. High-gain bidirectional converter with hybrid greylag goose optimization and quantum convolutional neural network for intelligent energy management in electric vehicle charging systems. Iran J Sci Technol Trans Electr Eng. 2025; 1-25. https://doi.org/10.1007/s40998-025-00991-3.
20. D. Selvaraj, S. Nattuthurai, A. Uehara, T. Senjyu, Optimal energy management strategy for electric vehicles and electricity distribution system based on quantile deep learning with enhanced African vulture optimization, Energy Rep. 2024;12:631–655. https://doi.org/10.1016/j.egyr.2024.06.016.
21. Mugemanyi S, Qu Z, Rugema FX, Dong Y, Bananeza C, Wang L. Marine predators algorithm: a comprehensive review. Mach Learn Appl. 2023; 12: 100471. https://doi.org/10.1016/j.mlwa.2023.100471.
22. Lalawat RS, Bajaj V, Padhy PK, Lin CY. Advancing motor imagery EEG classification by quantum feature integration and quantum support vector machines. Appl Acoust. 2025; 240: 110976. https://doi.org/10.1016/j.apacoust.2025.110976.
23. Liu J, et al. The road to quantum internet: progress in quantum network testbeds and major demonstrations. Prog Quantum Electron. 2025:100551. https://doi.org/10.1016/j.pquantelec.2024.100551.
24. Krishnan R. Electric motor drives: modeling, analysis, and control. 1st ed. New Jersey: Prentice Hall; 2001.
25. Antar RK, Saleh AA, Yahia TT. Estimate and control speed of a DC motor using different power circuits. Przegl Elektrotech. 2023; 99: 271-276. https://doi.org/10.15199/48.2023.03.48
26. Al-Hajzber SM, Al-Rifaie AH, Sultan NS. Intelligent techniques of design and comparative study for DC motor speed control fed by photovoltaic and fuel cells. J Adv Res Dyn Control Syst. 2018; 10: 1365-1376
27. Saleh HA, Alsaif OI, Abdulkadir LY. Adaptive control of a DC servo motor using particle swarm and gray wolf optimization algorithms. In: AIP Conference Proceedings. AIP Publishing.; 2025. https://doi.org/10.1063/5.0260224
28. Kavitha RJ, et al. Performance investigation of PI controller based chopper fed DC drive. Appl Mech Mater 2014; 573: 19-25. https://doi.org/10.4028/www.scientific.net/amm.573.19
29. Mohan N, Undeland TM, Robbins WP. Power electronics: converters, applications, and design. 3rd ed. Hoboken: Wiley; 2003.
30. Chapra SC, Canale RP. Numerical methods for engineers. New York: McGraw-Hill Higher Education; 2010.
31. Xu C, Zhang C, Xu M, Chen J, Wang L, Han Z. Improved active disturbance rejection speed tracking control for high-speed trains based on SBWO algorithm. Algorithms 2025;18:566. https://doi.org/10.3390/a18090566
32. Belguedri M, Benrabah A, Khoucha F, Benbouzid M, Benmansour K. An improved uncertainty and disturbance estimator-based speed control for grid-connected pumping kite wind generator. Control Eng Pract 2024; 143: 105795. https://doi.org/10.1016/j.conengprac.2023.105795
33. Gilbert EG, Kolmanovsky I, Tan KT. Discrete-time reference governors and the nonlinear control of systems with state and control constraints. Int J Robust Nonlinear Control 1995; 5: 487-504. https://doi.org/10.1002/rnc.4590050508
34. Han KH, Kim JH. Quantum-inspired evolutionary algorithm for a class of combinatorial optimization. IEEE Trans Evol Comput 2002; 6: 580-593. https://doi.org/10.1109/TEVC.2002.804320.
35. Garone E, Di Cairano S, Kolmanovsky I. Reference and command governors for systems with constraints: a survey on theory and applications. Automatica. 2017; 75: 306-328. https://doi.org/10.1016/j.automatica.2016.08.013.
36. Astrom KJ, Rundqwist L. Integrator windup and how to avoid it. In: American Control Conference. IEEE; 1989: 1693-1698. https://doi.org/10.23919/acc.1989.4790464.
37. Han KH, Kim JH. On setting the parameters of quantum-inspired evolutionary algorithm for practical applications. In: The 2003 Congress on Evolutionary Computation. IEEE. 2003: 178-184. https://doi.org/10.1109/cec.2003.1299572.
38. Vivek Y, Ravi V, Radha Krishna P. Quantum-inspired evolutionary algorithms for feature subset selection: a comprehensive survey. Quantum Inf Process. 2025; 24(7):1-44. https://doi.org/10.1109/cec.2003.1299572.
39. Vivek, Y., Ravi, V. & Krishna, P.R. Quantum-inspired evolutionary algorithms for feature subset selection: a comprehensive survey. Quantum Inf Process 24, 196 (2025). https://doi.org/10.1007/s11128-025-04787-6.
40. Anta RK, Suliman MY, Saleh AA. Harmonics resonance elimination technique using active static compensation circuit, Bull. Electr. Eng. Informatics. 2021;10:2405–2413. https://doi.org/10.11591/eei.v10i5.3148.

Omar Talal MAHMOOD received his B.Sc. from University of Technology, Iraq, M.Sc. from Northern Technical University, Iraq, and Ph.D. degree from UPM University, Malysia, in 1995, 2009, and 2025, respectively. He is currently an Assistant Professor at the Technical Engineering College, Northern Technical University, Mosul. His research interests and expertise include advanced control systems, power electronics, power quality, power converters and drives, and renewable energy systems.
e-mail: omar.talal@ntu.edu.iq

Laith A. MOHAMMED was born in Mosul/ Iraq He received an M.Sc. and Ph.D. Degree in electrical engineering from the University of Technology Bagdad –Iraq, University of Mosul –Iraq, in 2004 and 2017, respectively. Currently, he is an Assistant Professor in the Department of Electronic Power Techniques Engineering, at the Technical Engineering college of Mosul, Northern Technical University, his

research interests are power electronics, Power Quality, Renewable Energy systems, and Motor Drivers.
e-mail: laith.akram@ntu.edu.iq

Rakan Khalil ANTAR received his B.Sc., M.Sc., and Ph.D. degrees from the University of Mosul, Iraq, in 2002, 2005, and 2013, respectively. He is currently a Professor at the Technical Engineering College, Northern Technical University, Mosul. His research interests and expertise include power electronics, power quality, power converters and drives, and renewable energy systems.
e-mail: rakan.antar@ntu.edu.iq